NeptuniumV retention by siderite under anoxic conditions: Precipitation of NpO2–like nanoparticles and of NpIV pentacarbonate

Scheinost, A. C.; Steudtner, R.; Hübner, R.; Weiss, S.; Bok, F.;

Originally published:

September 2016

Environmental Science & Technology 50(2016)19, 10413-10420

DOI: https://doi.org/10.1021/acs.est.6b02399

Neptunium^{V} retention by siderite under anoxic conditions: Formation of nanoparticulate NpO_2 and Np^{IV} pentacarbonate

Andreas C. Scheinost[*,‡,§] *Robin Steudtner*[‡], *René Hübner*[†], *Stephan Weiss*[‡]

‡ Institute of Resource Ecology, Helmholtz-Zentrum Dresden - Rossendorf, D-01314, Germany

† Institute of Ion Beam Physics and Materials Research, Helmholtz-Zentrum Dresden - Rossendorf, D-01314, Germany

§ The Rossendorf Beamline at ESRF, F-38043 Grenoble, France

Abstract. The Np^{V} reactions with siderite, an Fe^{II} carbonate mineral with relevance for the near-field of high-level radioactive waste repositories, were investigated under anoxic conditions within the stability field of siderite (pH 7 to 13). Batch sorption experiments show that siderite has a high solid-water distribution coefficient ($logR_d$ >5) for aqueous $Np^{V}O_2^{+}$ across the investigated pH range. In comparison to the redox-inert carbonate calcite, this $logR_d$ is three orders of magnitude higher, and comparable to the $logR_d$ of the tetravalent actinide Th on calcite. Np L_3-edge X-ray absorption near-edge structure (XANES) spectroscopy confirmed that Np associated to siderite was reduced from the pentavalent to the tetravalent oxidation state. The local structure of the Np^{IV} phase, which was probed by extended X-ray absorption fine-structure (EXAFS) spectroscopy indicated the formation of NpO_2–like nanoparticles with diameter < 1 nm, further corroborated by high-resolution transmission electron microscopy (HR-TEM). The low solubility of these NpO_2–like nanoparticles, along with their negligible surface charge at neutral pH conditions which favors particle aggregation, suggest an efficient retention of Np in the near-field of

radioactive waste repositories. When Np^{V} was added to ferrous carbonate solution, the subsequent precipitation of siderite did not lead to a structural incorporation of Np^{IV} by siderite, but caused formation of Np^{IV} pentacarbonate, a hitherto enigmatic phase, while the penta-carbonates of U^{IV} and Pu^{IV} have been identified before.

Introduction

Nuclear power generation has left behind a legacy of high-level radioactive waste, which needs to be kept safe for hundreds of thousands of years. The disposal of this waste in deep geological formations behind multiple barriers is a concept favored by many power producing countries to ensure a lasting protection of people and the environment. The multiple barrier system consists of three principal parts, an engineered barrier (copper or stainless steel containers), a geo-engineered barrier (clay-based backfill-material, e.g. bentonite) and the geological barrier (argillaceous, granitic or salt host rock).[1] Many of these components contain or form Fe^{II}-bearing minerals, which may act as scavenger for potentially released radionuclides by their reducing power and sorption capacity. Steel containers are likely to corrode under near-field conditions, forming for instance magnetite, siderite, chukanovite and Fe-phyllosilicates in contact with clay backfill, [2, 3] magnetite and hydrous Fe^{II} oxides in contact with brine, [4] and Fe^{II} sulfides in the presence of sulfate reducing bacteria. [5] Such Fe^{II}-bearing minerals occur also naturally in clay rocks; e.g. MX80 bentonite considered as backfill material contains 0.7 % siderite and 0.3% pyrite, and Opalinus clay considered as host rock in Switzerland contains 6% siderite and 0.9% pyrite. [6, 7]

Spent nuclear fuel consists mainly of the original uranium dioxide (~95%) and its fission products (lanthanides, technetium, selenium, noble gases and cesium, ~4%). Neutron

absorption and decay reactions lead to the formation of plutonium isotopes (~1%) and the minor actinides neptunium, americium and curium (<0.1% of typical burnt fuel). The redox-sensitive elements uranium, plutonium, technetium, selenium have been shown to be efficiently immobilized by sorption and redox reactions on Fe^{II}-bearing minerals [4, 8-14] Much less work has been conducted on the redox-driven (anoxic) immobilization of the minor actinide neptunium, although its major radionuclide ^{237}Np has a very long half life (2.14 Mio years) and contributes significantly to the long-term radiotoxicity of spent fuel. Work attempting to elucidate the mechanisms of Np reduction by mineral surfaces is even more scarce. Np^{V} was found to be much more strongly retained by magnetite under anoxic conditions than under normal atmosphere; using a liquid extraction technique, Np associated with the solid phase was determined to be tetravalent. [15] In comparison to aqueous Fe^{II}, the reduction by magnetite was 3 orders of magnitude faster. [16] A pioneering study employing EXAFS spectroscopy showed that Np^{V} was only weakly taken up by mackinawite, forming rather surprisingly a mononuclear Np^{IV} sorption complex coordinated to both O and S. [17] In the presence of green rust, Np^{V} was rapidly sorbed and reduced to Np^{IV} at the edges of the hexagonal platelets; the authors suggest formation of Np^{IV} particles, but their identification by TEM remained elusive. [18] Np^{V} reacted with Opalinus clay was reduced to Np^{IV} and showed a strong association with pyrite particles embedded in the clay matrix; the exact nature of the reduced Np^{IV} could not be identified, but the authors excluded formation of NpO_2 due to the absence of Np-Np backscattering contributions in Np L_3-edge EXAFS spectra. [19] Biotite and chlorite with structural Fe^{II} fully reduced Np^{V} to Np^{IV}, and nanoparticulate NpO_2 formed as identified by EXAFS. [20] In the presence of Ti-doped magnetite, sorption of Np^{V} was high at pH values 5 and 7, while the sorption at pH 3 was low, but increased with Ti-doping most likely because of the increasing Fe^{II} fraction to counterbalance the charge of structural Ti^{IV}. Using Np L_3-edge XANES and EXAFS, the

reaction product could be identified as a Np^{IV} species, while the absence of Np-Np backscattering contradicted formation of NpO_2. [21] The authors claim formation of an innersphere sorption complex, but fitted Np-Fe and Np-Ti coordination numbers between 5 and 7 would rather suggest structural incorporation by magnetite or a secondary Fe phase. In conclusion, the few studies on Np uptake by Fe^{II}-bearing minerals under anoxic conditions show sorption and reduction to Np^{IV}, but the reaction mechanism and the end product, i.e. sorption complexation vs. structural incorporation vs. NpO_2 precipitation, often remain elusive.

The objective of our study was therefore, to investigate the Np reduction products under strictly anoxic atmosphere by a combination of Np L_3-edge XAFS spectroscopy and electron microscopy. As Fe^{II}-bearing mineral phase, the Fe^{II} carbonate siderite was selected because of its relevance for many high-level radioactive waste scenarios as outlined above. The extent of reduction as well as the reduction kinetics of siderite (or the hydroxocarbonate chukanovite) are smaller than that of other Fe^{II}-bearing minerals, most likely because of a larger bandgap preventing a free electron flow from the structure, and also because dissolved carbonate might form complexes with Fe^{II} and the oxidant, thereby potentially competing with the Fe-oxidant redox reaction. Nevertheless, siderite reduced Se^{IV} to elemental selenium, and Pu^{V} to $Pu^{IV}O_2$-like solids, hence we expected that Np^{V} would also be reduced by siderite. [11, 22]

Materials and Methods

Caution! *^{237}Np is a radioactive isotope and an α-emitter. It should be handled in dedicated facilities with appropriate equipment for radioactive materials to avoid health risks caused by radiation exposure.*

Generally, all sample manipulations, including mineral synthesis and washing, UV-vis measurements, and preparation of samples for XAS measurements, were carried out under anoxic conditions in a nitrogen glove-box with 0 – 5 ppmv O_2. Experiments were carried out at RT (23 ± 3°C); deionized (18.2 MΩ cm Milli-Q), degassed (O_2 and CO_2 free) water was used for all purposes.

Siderite synthesis and characterization. A siderite ($Fe^{II}CO_3$) suspension ([Fe_{tot}] = 0.2 M) was prepared by slowly mixing 100 mL of a 0.4 M $Fe^{II}Cl_2$ solution with 100 mL of a 0.8 M Na_2CO_3 solution [23]. The light gray precipitate was washed with 0.1 M NaCl (at least 3 washing cycles) and kept in suspension in 0.1 M NaCl. Siderite is extremely oxidation-sensitive and not stable in suspension with an ionic strength lower than 0.1 M, as indicated by the rapid appearance of brownish Fe^{III} oxyhydroxides like goethite.[24, 25] Raman spectroscopic measurements were carried out with a Raman-microscope (HORIBA Jobin Yvon LabRAM Aramis Vis) using an Argon-Laser (437 nm) with an output energy of 0.2 mW as light source and confirmed the phase identity and purity (see Fig. S1 in SI). An isoelectric point at 10.1 was determined by zeta potential measurements using a Laser-Doppler-Electrophoresis instrument (Zetasizer nano-ZS, Malvern Instruments Ltd.) (Fig. S2).

Np(V) stock solution. A 0.056 M Np^V stock solution in 1.0 M $HClO_4$ was prepared from neptunium (^{237}Np) dioxide (CEA-Marcoule, France), according to a previously reported procedure [26]. The pentavalent oxidation state of Np was prepared by electrochemical reduction from Np^{VI} and verified by UV-VIS-NIR spectroscopy. This solution was diluted with degassed deionized water to obtain a stock solution of 10^{-3} M Np^V.

Batch sorption. The Np^V retention by $Fe^{II}CO_3$ was investigated in the pH range 7 to 13 by batch experiments. For pre-equilibration, $Fe^{II}CO_3$ suspensions (S/L ratio of 1 g/L) were prepared in 0.1 M NaCl background electrolyte and continuously shaken on a horizontal

shaker for 48 h, with pH values initially adjusted and readjusted if necessary. Then, aliquots of the Np^{V} stock solution were added to the $Fe^{II}CO_3$ suspensions to obtain the final Np^{V} concentration of $2 \cdot 10^{-5}$ M. The pH values were readjusted immediately. For sorption, the samples were shaken on a horizontal shaker up to 3 weeks, whereby the pH was monitored and readjusted if necessary. Finally, the remaining suspensions were centrifuged for phase separation (60 min, 3200×g). The final Np concentration in the supernatant was determined by liquid scintillation counting (LSC, Winspectral α/β, Wallac 1414, Perkin Elmer) using α-β discrimination with a lower detection limit of $\leq 10^{-9}$ M. The distribution coefficient R_d in L/kg was calculated with

$$R_d = \frac{c_{ini} - c_{eq}}{c_{eq}} \cdot \frac{V}{m},$$

where c_{ini} and c_{eq} (mol/L) are the initial and equilibrium Np concentration in solution, V (L) the sample volume and m (kg) the mass of siderite.

Np siderite coprecipitation. In addition to the batch sorption experiments, where Np^{V} was added to pre-synthesized siderite, we also conducted a Np^{V}-siderite coprecipitation experiment to study the eventual structural incorporation of Np. This experiment was performed like the pure mineral synthesis described before, except that an appropriate aliquot of the Np stock solution to obtain a nominal loading Np/siderite of 4705 mg/kg was slowly added to the $Fe^{II}Cl_2$ solution, before adding the Na_2CO_3 solution to initiate the siderite precipitation.

X-ray absorption spectroscopy. We selected a sorption time series at pH 7.7 ±0.3, i.e. in the pH range of the lowest siderite solubility, [27] at ionic strength of 0.1 M and after reaction times of 1 h, 1 d, 7 d and 21 d, two additional sorption samples at the same pH, a reaction time of 7 d, and an ionic strength of 0.001 and 1 M, and the coprecipitation sample (Table S1). After

phase separation by centrifugation, the solids were filled into double-confinement, heat-sealed polyethylene sample holders inside the anoxic glovebox. The samples were then removed from the glovebox and immediately flash-frozen in LN_2 and stored in an LN_2 dewar to prevent oxygen diffusion into the samples and to freeze-in chemical reactions until XAS measurements. After transport to the Rossendorf Beamline at ESRF (Grenoble, France), the samples were individually removed from the LN_2 dewar and transferred to a closed-cycle He cryostat operating at 10 K within less than 30 sec for XAS measurements. XAS (XANES and EXAFS) measurements were carried out in fluorescence mode at the Np– L_{III} edge (17610 eV) using a 13-element high-purity Ge solid state detector (Canberra) with digital signal analysis (XIA XMap). The polychromatic synchrotron beam was monochromatized using a pair of water-cooled Si(111) crystals, and higher-order harmonics were rejected by a Rh-coated 1.3-m long collimating mirror before the double-crystal monochromator, and a 1.2-m long Rh-coated toroidal mirror after the monochromator. Between 6 and 12 individual XAS scans were energy-calibrated against a simultaneously measured Y foil (17038 eV), corrected for fluorescence deadtime and averaged using the SIXpack, [28] while subsequent data reduction steps and shell fits were conducted using WinXAS. [29] Theoretical backscattering paths were calculated with FEFF8.2 using crystal structures of NpO_2 and siderite (with one Fe replaced by Np). [30-32] Reference spectra for the Np^{IV} aquo complex [33] and for NpO_2 [34]were downloaded from AcReDaS, the online actinide reference database for spectroscopy. [35]

Transmission electron microscopy (TEM). A sample ($[Np^V]_{ini}$ = $2 \cdot 10^{-5}$ M, s/l = 0.1 $g \cdot L^{-1}$, I = 0.1 M (NaCl), reacted for 7 d under anoxic conditions) was prepared by disposing a drop of the Np-siderite suspension on a carbon-coated copper grid (400 mesh, S 160, Plano GmbH) and drying it under an inert gas atmosphere. Bright-field TEM and high-resolution TEM (HRTEM) images were collected on an image C_s-corrected Titan 80-300 electron microscope (FEI) operated at 300 kV. Selected area electron diffraction (SAED) patterns

were acquired from a specimen area of 190 nm in diameter. Energy-dispersive X-ray spectroscopy (EDXS) was performed in scanning TEM mode with a Li-drifted silicon detector (EDAX).

Results and discussion

The Np^{V} uptake by siderite is very high with $logR_d$ values always above 5 and little variation across the pH range 7 to 13 (Fig. 1 top)). In comparison to the Np^{V} uptake by the (redox-inactive) carbonate calcite, these $logR_d$ values are three orders of magnitude higher, [36] and much more similar to values obtained for the tetravalent actinide, Th, on calcite, [37] in both cases at comparable pH. Hence the high $logR_d$ values are a first indication that Np^{V} was indeed reduced to Np^{IV} by siderite. Further support comes from by the thermodynamic calculation, showing that at the measured Eh values at pH 8, 10 and 12, the equilibrium should be dominated by NpO_2 (Fig. 1 bottom).

Figure 2 shows the Np-L_{III} edge XANES spectra of the siderite sorption time series at pH 7.7 ±0.3, and of the coprecipitation sample. All spectra are well aligned and correspond both in edge and white-line position with the two Np^{IV} references, NpO_2 and an Np^{IV} aquo complex. [33, 34] This is further confirmed by the XANES edge energies as determined by the knot of the second derivative, which vary by less than 0.3 eV from the average of 17613.5 eV (Table 1). Therefore, Np^{V} is fully reduced to Np^{IV} in all systems, even already after the shortest sorption time of 1 h, and also in the coprecipitation sample.

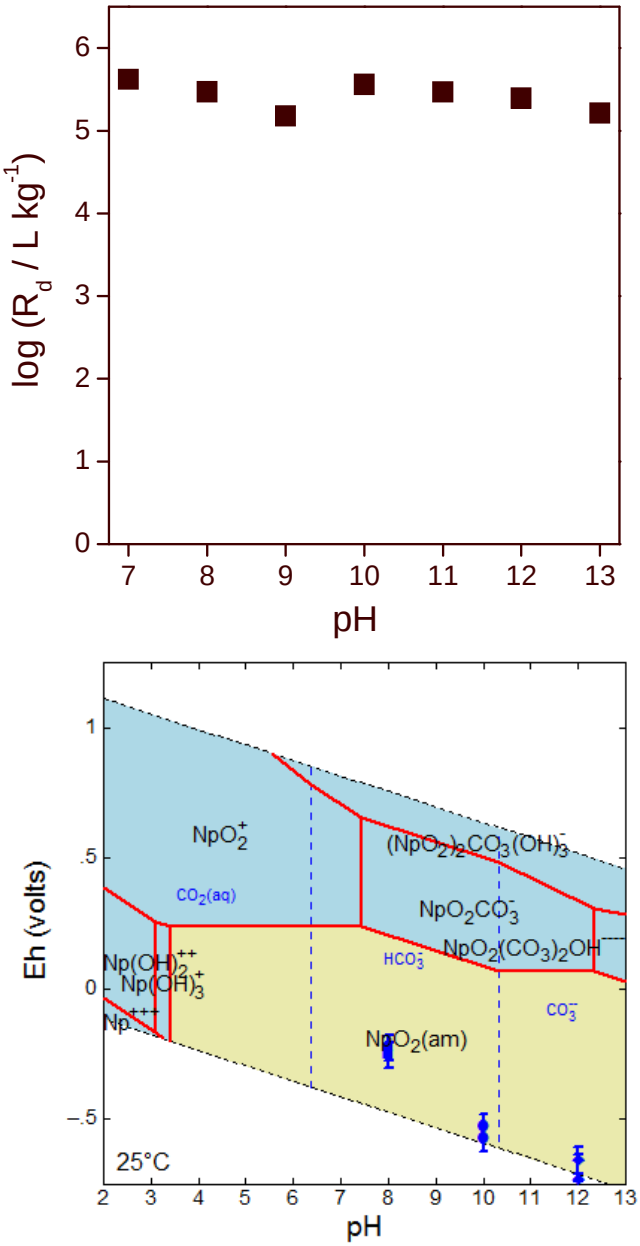

Figure 1. Top: Np solid/liquid distribution coefficient in the siderite system as function of pH. $[Np^V]_{initial}$ = $2 \cdot 10^{-5}$ M, s/l = 1 g·L^{-1}, I = 0.1 M NaCl, after 1 week reaction time under anoxic N_2. Bottom: Eh-pH diagram calculated for the chemical system 2 10^{-5} M Np^V in 0.1 M NaCl solution in presence of siderite under anoxic conditions at 25°C. Thermodynamic data of the Lawrence Livermore National Laboratory thermo database were supplemented by the most recent NEA database. [38, 39]Experimental results represented by blue symbols for the batch experiments.

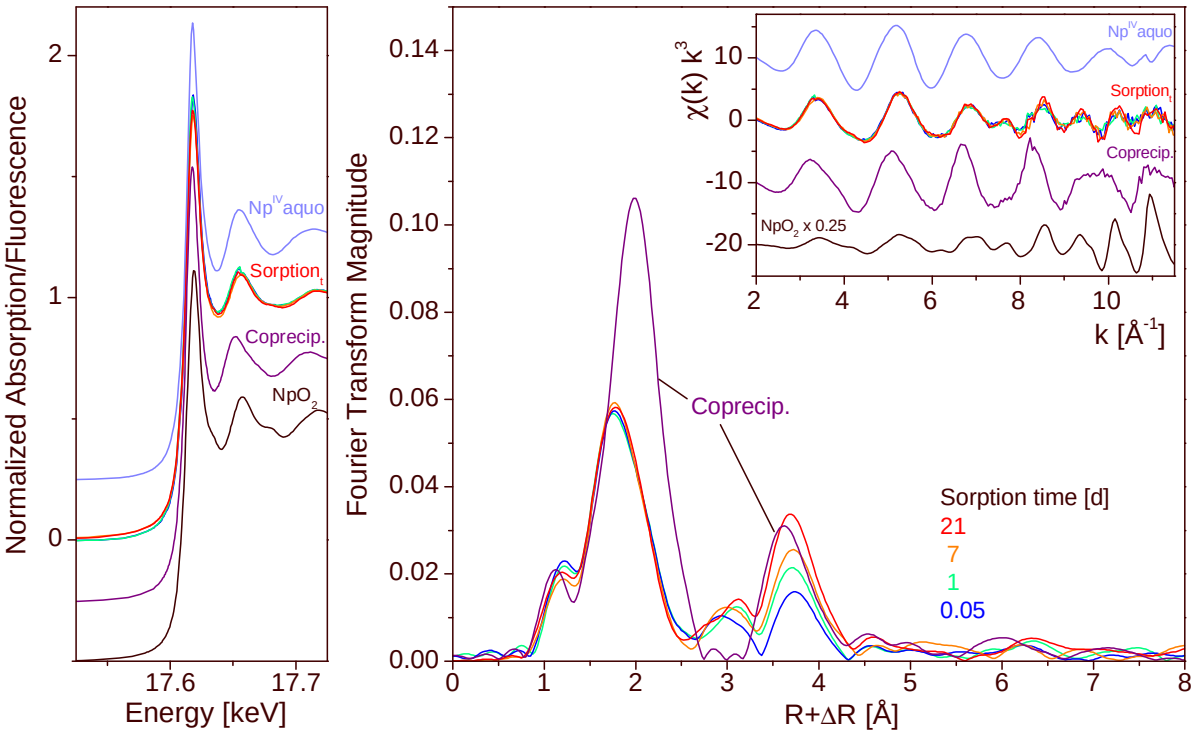

Figure 2. Neptunium L_{III}-edge XAS spectra of selected siderite sorption and coprecipitation samples (pH 7.7 ± 0.3) along with Np references. Left: XANES spectra, right: EXAFS Fourier transform magnitude and corresponding χ(k) spectra as insert.

The EXAFS Fourier transform magnitudes of the sorption samples show a coordination shell at R+ΔR=1.8 Å (uncorrected for phase shift), which is fitted by about 8 oxygen atoms at a distance of 2.34 – 2.35 Å. Note that the small peak at the left side of this coordination shell cannot be fitted with a Np-O distance of 1.87 Å as would be expected for the –yl group of Np^{V}; they constitute instead a truncation artifact of the Fourier transformation arising from the relatively short k-range. A second peak at R+ΔR=3.7 Å increases in height with sorption time. Wavelet analysis of this peak reveals an amplitude maximum at k>10 $Å^{-1}$, in line with backscattering by a heavy element. [40] Correspondingly, this shell could be fitted with Np atoms at a distance of 3.82 – 3.84 Å.

Table 1. Np-L_{III} XANES edge energies and EXAFS fit results of Np siderite samples and references (S_0^2=0.9, fit range 2.0 – 11.5 Å^{-1}).

Sample	E_0 [eV]	First shell			Second shell				ΔE_0 [eV]	χ^2_{res} %
		CN[1]	R[2] [Å]	σ[2,3] [Å]	CN		R [Å]	σ [Å^2]		
Sorption 1 h (0.1 M)	17613.3	8.0 O	2.35	0.0100	2.1 Np		3.83	0.0026	7.1	19.3
Sorption 1 d (0.1 M)	17613.4	7.7 O	2.35	0.0100	4.4 Np		3.84	0.0100	7.6	19.8
Sorption 7 d (0.1 M)	17613.3	7.8 O	2.34	0.0100	3.9 Np		3.83	0.0054	7.4	16.4
Sorption 21 d (0.1 M)	17613.5	7.9 O	2.34	0.0100	3.8 Np		3.82	0.0034	7.0	13.8
Sorption 0.001 M (7 d)	17613.6	8.4 O	2.35	0.0100	3.4 Np		3.83	0.0027	7.4	14.6
Sorption 1 M (7 d)	17613.6	8.0 O	2.34	0.0100	3.6 Np		3.83	0.0060	7.3	15.5
Sid-coprecipitate	17613.8	9.6 O	2.41	0.0048	4.2	C_{bid}	2.87	0.0010	14.6	12.8
					4.2[c]	O_{dist}	4.14[c]	0.0016[c]		
					8.4[2c]	C_{bid}-O_{dist}	4.14[c]	0.0016[c]		
					4.2[c]	C_{bid}-O_{dist}-C_{bid}	4.14[c]	0.0016[c]		
Np^{IV}aquo	17613.8	11.6 O	2.39	0.0083					9.4	5.2
NpO_2	17613.6	8 O	2.35	0.0043	12	Np	3.85	0.0010	9.6	19.4
					24 O		4.48	0.0010		
NpO_2 crystal structure[41]		8 O	2.35		12	Np	3.84			
					24 O		4.51			

[1] CN: coordination number, error ± 25 %

[2] R: Radial distance, error ±0.01 Å

[3] σ2: Debye-Waller factor, error ±0.0005 Å^2

The interatomic distances (R) for these nearest Np–O and Np–Np shells are close to those of NpO_2. While the coordination numbers (CN) for the Np-O shell are close to 8 as in the cubic NpO_2 structure, the CNs of the Np-Np path are much lower with larger Debye–Waller factors

(σ^2) as compared with those for NpO_2. [41] A NpO_2 cluster with 1 nm diameter contains 13 Np atoms with an average Np-Np coordination number of 5.5 (12×5+1×12). This coordination number is significantly higher than the ones derived from EXAFS shell fit (3.5 per average for all sorption samples), suggesting an even smaller average particle size, or cation vacancies. Similar trends were observed for nanocrystalline Np dioxide particles formed after dilution of aqueous Np^{IV} carbonate complexes [34] and for other An^{IV} oxide/hydroxide species. [42-44] Therefore, the EXAFS analysis suggests that Np^{V} reduction at the siderite surface leads to the formation of either small particles of crystalline NpO_2 or to structurally disordered Np^{IV} oxide/hydroxide. While the peak height of the Np-Np shell increases with increasing sorption time, suggesting the growth of nanoparticles with time, the shell fit data suggest a more complicated process: between 1 h and 1 d sorption time, the CN doubles from 2 to 4, but then remains constant. At the same time, the Debye-Waller factor increases from 0.0026 to 0.0100 $Å^2$, and decreases thereafter with increasing sorption time to 0.0034 $Å^2$. This suggests that the initial particles are small, but well ordered, and then grow with high disorder, which subsequently obtain a higher degree of order with sorption time. Ionic strength of the background electrolyte also shows a significant effect on the Debye-Waller factor, which increases from 0.0027 to 0.0054 to 0.0060 $Å^2$, when the ionic strength increases from 0.001 to 0.1 to 1 M for a constant reaction time of 7 d. Therefore, increasing background electrolyte concentrations seem to increasingly interfere with the crystallization process.

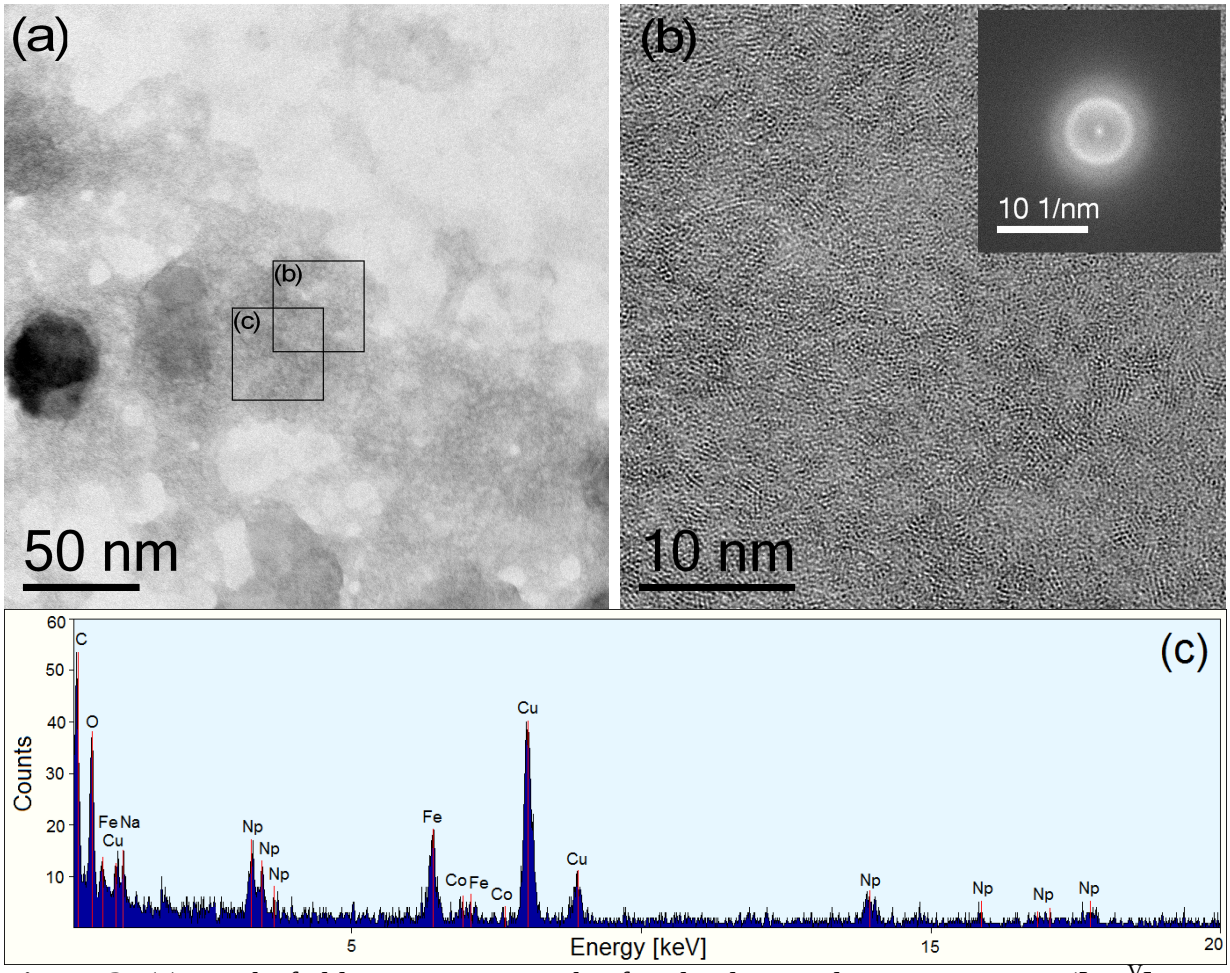

Figure 3. (a) Bright-field TEM micrograph of a dried Np siderite suspension ($[Np^{V}]_{ini}$ = $2 \cdot 10^{-5}$ M, s/l = 0.1 g·L^{-1}, pH=7.6, I = 0.1 M (NaCl), after 7 d under anoxic conditions). (b) HR-TEM image of area (b). (c) Energy-dispersive X-ray (EDX) spectrum obtained in scanning TEM mode from the area (c).

To further characterize its microstructure, a dried Np siderite suspension was analyzed using TEM. A corresponding bright-field TEM micrograph is shown in Fig. 3a. While the black particle with a diameter of approximately 40 nm is siderite, the gray areas arise from particles much smaller than siderite. According to the HRTEM image shown in Fig. 3b, their average size is in the order of ≤ 1 nm. Corresponding to this small particle size, the Fourier transform in the inset does not show sharp distinctive rings. The dominant presence of Np and O determined in an adjacent region by energy-dispersive X-ray (EDX) spectroscopy (Fig. 3c) confirms that these small particles constitute indeed the Np phase (Note that C and Cu stem

from the TEM support grid, and Fe and Co from the objective lens pole piece; however, a contribution of siderite to the Fe fluorescence line cannot be excluded). Extended electron irradiation (1-2 min.) induced particle growth, and selected area electron diffraction of those irradiated regions led to diffraction patterns with distinctive diffraction rings which are in agreement with the fluorite-type NpO_2 structure ($Fm\bar{3}m$) (not shown here). [45] Thus, the TEM investigations support the EXAFS analysis that Np^{IV} is precipitated as precursor of nanoparticulate NpO_2 with particle sizes below 1 nm.

In contrast to the sorption samples, the EXAFS Fourier transform magnitude of the coprecipitation sample shows a much higher and more distant coordination shell (Fig. 2 right), which could be fitted with ~10 oxygen atoms at a distance of 2.41 Å, i.e. not commensurate to the cubic NpO_2 structure (Table 1). Furthermore, the second shell is at a shorter distance than the Np-Np shell of NpO_2. Wavelet analysis of this shell shows a maximum of k at about 8 $Å^{-1}$, hence discards that this peak arises from Np-Np backscattering. The spectrum is in fact similar to compounds where carbon is bidentately coordinated, like in Ce^{IV} or U^{IV} carbonate compounds. [46] This was confirmed by a shell fit based on this bidentate arrangement, which gives rise to very characteristic multiple scattering paths involving the nearest C_{bid} and the next nearest, distal O (O_{dist}) atom of the carbonate molecule. The Np-O coordination number of ~10 as well as the Np-C_{bid} coordination number of 4.2 (theoretically 5) confirm the formation of $Np^{IV}(CO_3)_5$ units very similar to those found for U^{IV} and Pu^{IV} before, and in line with the similar complex formation constants of all three actinides. [46-48] As expected for the slightly smaller ionic radius of Np^{IV} versus U^{IV}, the fitted distances are about 0.02 Å shorter than for the U^{IV} carbonate unit (Table 1). Analogous to U^{IV}, the Np^{IV} pentacarbonate unit may exist either as aquo-anion complex, [34] or in the solid state with e.g. Na for charge compensation and crystal water. [46] The relatively strong association of this

257 Np^{IV} species with the solid phase ($logR_d$=4.0) leaves little doubt about the solid-state nature
258 of this Np^{IV} carbonate species, since the potentially 6-fold negative charge of the aquo-anion
259 would prevent strong sorption to the siderite surface. Furthermore, a fit of the spectrum
260 assuming that Np^{IV} resides in the octahedrally coordinated position of Fe^{II} in siderite failed
261 due to the fact that no Np-C shell at a distance of 3.0 to 3.4 Å could be fitted, which would be
262 characteristic for the monodentate coordination of carbon and the cations in siderite.
263 Therefore, our results demonstrate that Np^{IV} does not form part of the siderite structure
264 through co-precipitation, but is entrapped by formation of a Np^{IV} carbonate precipitate.
265 Evidently, the strong complexation of Np with dissolved carbonate prevented the
266 incorporation by siderite. [48]

267

268

269 ## Environmental implications

270 After reaction of Np^{V} with siderite, we could demonstrate for the first time the formation of
271 NpO_2-like nanoparticles, while formation of (a significant amount of) monomeric Np^{IV}
272 sorption complexes could be excluded. The formation of a NpO_2-like phase by a surface-
273 mediated redox reaction is in line with results by a recent study showing Np^{V} reduction by
274 biotite and chlorite with reduced structural iron. [20] It is also in line with formation of UO_2–
275 like nanoparticles upon U^{VI} sorption to e.g. magnetite and mackinawite. [49, 50] Interestingly,
276 the strong affinity of Np^{IV} towards carbonate did not prevent the precipitation of the NpO_2-
277 like phase, likewise to the formation of PuO_2 after reaction of Pu^{V} with the Fe^{II}
278 hydroxocarbonate chukanovite. [11] This can be explained by the relatively low siderite
279 solubility in the investigated pH range. Only when Np^{V} was added to the 0.8 M carbonate
280 solution prior to siderite precipitation, strong carbonate complexation and subsequent

281 precipitation of a Np^{IV} pentacarbonate took place. Since such high carbonate concentrations
282 are not to be expected under radioactive waste conditions, formation of NpO_2-like
283 nanoparticles is certainly more relevant for the safety case.

284 The observed high retention of Np by siderite across a relatively wide pH range is
285 encouraging. However, the potential mobilization of the formed NpO_2–like nanoparticles as
286 colloids may significantly raise the risk of Np migration away from the waste disposal site. [51,
287 52] The two-electron transition from U^{VI} to U^{IV} requires the formation of a chemical bond with
288 an electron-providing surface, while the formation of aqueous Fe-U ion pairs can provide
289 only one electron, which kinetically hinders the redox reaction. [53] Not surprizingly, TEM
290 images of surface-catalyzed UO_2 show an intimate spatial association with the mineral
291 surface. [49, 50] This is not the case for the NpO_2 particles, which are diffusely distributed
292 between the siderite particles (Fig. 3 a), thereby suggesting that the single electron required
293 for the Np^{V} reduction might be provided by dissolved Fe^{II} species. This is further supported
294 by the high isoelectric point of siderite (pH 10.1), leading to charge repulsion between the
295 (net) positively charged surface and the cationic $Np^{V}O_2^{+}$ species prevailing below pH 10,
296 which should also favor a redox reaction between dissolved Np^{V} and Fe^{II} species. Therefore,
297 the NpO_2–like nanoparticles formed in presence of siderite may have a significant tendency
298 to become detached from the mineral assembly. This does not necessarily mean that they also
299 have a strong tendency to form mobile colloids, since their surface charge is low at
300 circumneutral conditions, which favors their coagulation and causes a relatively fast settling.
301 [34] This, however, may change in the presence of dissolved silica, since then amorphous NpO_2
302 silica structures can form, whose negatively-charged silanol surface groups may provide
303 rather stable colloidal suspensions. [54]

304

Author information

Corresponding Author

*Phone: ++33 476 88 2462. E-mail: scheinost@esrf.fr

Notes

The authors declare no competing financial interest.

Acknowledgments

This work funded by BMWi (02NUK019D, IMMORAD). We thank the ROBL team, and Maria Berger, Anika Maffert, Christa Müller, Ina Kappler and Sophia Kostudis for their invaluable help. Support by the Ion Beam Center (IBC) at HZDR is gratefully acknowledged. Paul Wersin (University of Berne) has performed the thermodynamic calculations given in SI.

References

(1) Sellin, P.; Leupin, O. X. The use of clay as an engineered barrier in radioactive waste management - A review. *Clays and Clay Minerals* **2013,** *61* (6), 477-498.

(2) Schlegel, M. L.; Bataillon, C.; Blanc, C.; Pret, D.; Foy, E. Anodic activation of iron corrosion in clay media under water-saturated conditions at 90 degrees C: Characterization of the corrosion interface. *Environmental Science & Technology* **2010,** *44* (4), 1503-1508.

(3) Wersin, P.; Jenni, A.; Mader, U. K. Interaction of corroding iron with bentonite in the ABM1 experiment at Aspo, Sweden: A microscopic approach. *Clays and Clay Minerals* **2015,** *63* (1-2), 51-68.

(4) Grambow, B.; Smailos, E.; Geckeis, H.; Muller, R.; Hentschel, H. Sorption and reduction of uranium(VI) on iron corrosion products under reducing saline conditions. *Radiochimica Acta* **1996,** *74*, 149-154.

(5) El Hajj, H.; Abdelouas, A.; El Mendili, Y.; Karakurt, G.; Grambow, B.; Martin, C. Corrosion of carbon steel under sequential aerobic-anaerobic environmental conditions. *Corrosion Science* **2013,** *76*, 432-440.

(6) Marques Fernandes, M.; Ver, N.; Baeyens, B. Predicting the uptake of Cs, Co, Ni, Eu, Th and U on argillaceous rocks using sorption models for illite. *Applied Geochemistry* **2015,** *59*, 189-199.

(7) Karnland, O. *Chemical and mineralogical characterization of the bentonite buffer for the acceptance control procedure in a KBS-3 repository*; Technical Report SKB TR-10-60: 2010.

(8) Myneni, S. C. B.; Tokunaga, T. K.; Brown, G. E. Abiotic selenium redox transformations in the presence of Fe(II,III) oxides. *Science* **1997,** *278*, 1106-1109.

(9) Scheinost, A. C.; Charlet, L. Selenite reduction by mackinawite, magnetite and siderite: XAS characterization of nanosized redox products. *Environ. Sci. Technol.* **2008,** *42* (6), 1984–1989.

(10) Jaisi, D. P.; Dong, H.; Plymale, A. E.; Fredrickson, J. K.; Zachara, J. M.; Heald, S.; Liu, C. Reduction and long-term immobilization of technetium by Fe(II) associated with clay mineral nontronite. *Chemical Geology* **2009,** *264* (1-4), 127-138.

(11) Kirsch, R.; Fellhauer, D.; Altmaier, M.; Neck, V.; Rossberg, A.; Fanghänel, T.; Charlet, L.; Scheinost, A. C. Oxidation state and local structure of plutonium reacted with magnetite, mackinawite and chukanovite. *Environ. Sci. Technol.* **2011,** *45* (17), 7267–7274.

(12) Um, W.; Chang, H.-S.; Icenhower, J. P.; Lukens, W. W.; Serne, R. J.; Qafoku, N. P.; Westsik, J. H., Jr.; Buck, E. C.; Smith, S. C. Immobilization of 99-Technetium (VII) by Fe(II)-Goethite and Limited Reoxidation. *Environmental Science & Technology* **2011,** *45* (11), 4904-4913.
(13) Huber, F.; Schild, D.; Vitova, T.; Rothe, J.; Kirsch, R.; Schafer, T. U(VI) removal kinetics in presence of synthetic magnetite nanoparticles. *Geochim. Cosmochim. Ac.* **2012,** *96*, 154-173.
(14) Peretyazhko, T. S.; Zachara, J. M.; Kukkadapu, R. K.; Heald, S. M.; Kutnyakov, I. V.; Resch, C. T.; Arey, B. W.; Wang, C. M.; Kovarik, L.; Phillips, J. L.; Moore, D. A. Pertechnetate (TcO4-) reduction by reactive ferrous iron forms in naturally anoxic, redox transition zone sediments from the Hanford Site, USA. *Geochimica Et Cosmochimica Acta* **2012,** *92*, 48-66.
(15) Nakata, K.; Nagasaki, S.; Tanaka, S.; Sakamoto, Y.; Tanaka, T.; Ogawa, H. Sorption and reduction of neptunium(V) on the surface of iron oxides. *Radiochimica Acta* **2002,** *90* (9-11), 665-669.
(16) Nakata, K.; Nagasaki, S.; Tanaka, S.; Sakamoto, Y.; Tanaka, T.; Ogawa, H. Reduction rate of neptunium(V) in heterogeneous solution with magnetite. *Radiochimica Acta* **2004,** *92* (3), 145-149.
(17) Moyes, L. N.; Jones, M. J.; Reed, W. A.; Livens, F. R.; Charnock, J. M.; Mosselmans, J. F. W.; Hennig, C.; Vaughan, D. J.; Pattrick, R. A. D. An X-ray absorption spectroscopy study of neptunium(V) reactions with mackinawite (FeS). *Environ. Sci. Technol.* **2002,** *36* (2), 179-183.
(18) Christiansen, B. C.; Geckeis, H.; Marquardt, C. M.; Bauer, A.; Roemer, J.; Wiss, T.; Schild, D.; Stipp, S. L. S. Neptunyl (NpO2+) interaction with green rust, GR(Na,SO4). *Geochimica Et Cosmochimica Acta* **2011,** *75* (5), 1216-1226.
(19) Frohlich, D. R.; Amayri, S.; Drebert, J.; Grolimund, D.; Huth, J.; Kaplan, U.; Krause, J.; Reich, T. Speciation of Np(V) uptake by Opalinus Clay using synchrotron microbeam techniques. *Anal. Bioanal. Chem.* **2012,** *404* (8), 2151-2162.
(20) Brookshaw, D. R.; Pattrick, R. A. D.; Bots, P.; Law, G. T. W.; Lloyd, J. R.; Mosselmans, J. F. W.; Vaughan, D. J.; Dardenne, K.; Morrie, K. Redox Interactions of Tc(VII), U(VI), and Np(V) with Microbially Reduced Biotite and Chlorite. *Environmental Science & Technology* **2015,** *49* (22), 13139-13148.
(21) Wylie, E. M.; Olive, D. T.; Powell, B. A. Effects of Titanium Doping in Titanomagnetite on Neptunium Sorption and Speciation. *Environmental Science & Technology* **2016,** *50* (4), 1853-1858.
(22) Scheinost, A. C.; Kirsch, R.; Banerjee, D.; Fernandez-Martinez, A.; Zaenker, H.; Funke, H.; Charlet, L. X-ray absorption and photoelectron spectroscopy investigation of selenite reduction by FeII-bearing minerals. *J. Contam. Hydrol.* **2008,** *102* (3-4), 228-245.
(23) Charlet, L.; Wersin, P.; Stumm, W. Surface-charge of $MnCO_3$ and $FeCO_3$. *Geochim. Cosmochim. Acta* **1990,** *54* (8), 2329-2336.
(24) Postma, D. Pyrite and siderite oxidation in swamp sediments. *Journal of Soil Science* **1983,** *34* (1), 163-182.
(25) Scheinost, A. C.; Schwertmann, U. Color identification of iron oxides and hydroxysulfates - Use and limitations. *Soil Science Society of America Journal* **1999,** *63*, 1463-1471.
(26) Ikeda-Ohno, A.; Hennig, C.; Rossberg, A.; Funke, H.; Scheinost, A. C.; Bernhard, G.; Yaita, T. Electrochemical and complexation behavior of neptunium in aqueous perchlorate and nitrate solutions. *Inorganic Chemistry* **2008,** *47* (18), 8294-8305.
(27) Bruno, J.; Wersin, P.; Stumm, W. On the influence of carbonate in mineral dissolution. 2. The solubility of $FeCO_3$(s) at 25-degrees-C and 1 atm total pressure. *Geochimica et Cosmochimica Acta* **1992,** *56* (3), 1149-1155.
(28) Webb, S. M. SIXpack: a graphical user interface for XAS analysis using IFEFFIT. *Physica Scripta* **2005,** *T115*, 1011-1014.
(29) Ressler, T. WinXAS: a program for X-ray absorption spectroscopy data analysis under MS-Windows. *Journal of Synchrotron Radiation* **1998,** *5*, 118-122.
(30) Ankudinov, A. L.; Rehr, J. J. Relativistic calculations of spin-dependent x-ray-absorption spectra. *Physical Review B* **1997,** *56*, 1712-1728.
(31) Benedict, U.; Dabos, S.; Dufour, C.; Spirlet, J. C.; Pages, M. Neptunium compounds under high pressure. *Journal of the Less-Common Metals* **1986,** *121*, 461-468.
(32) Effenberger, H.; Mereiter, K.; Zemann, J. Crystal-structure refinements of magnesite, calcite, rhodochrosite, siderite, smithonite, and dolomite, with discussion of some apsctes of the stereochemistry of calcite-type minerals. *Zeitschrift fur Kristallographie* **1981,** *156* (3-4), 233-243.
(33) Hennig, C. Evidence for double-electron excitations in the L_3-edge x-ray absorption spectra of actinides. *Phys. Rev. B* **2007,** *75* (035120), 035120-1 - 035120-7.

(34) Husar, R.; Hübner, R.; Hennig, C.; Martin, P. M.; Chollet, M.; Weiss, S.; Stumpf, T.; Zänker, H.; Ikeda-Ohno, A. Intrinsic formation of nanocrystalline neptunium dioxide under neutral aqueous conditions relevant to deep geological repositories. *Chemical Communications* **2015,** *51* (7), 1301-1304.
(35) Rossberg, A.; Scheinost, A. C.; Schmeisser, N.; Rothe, J.; Kaden, P.; Schild, D.; Wiss, T.; Daehn, R. AcReDaS, an Actinide Reference Database for XAS, EELS, IR, Raman and NMR Spectroscopy. In http://www.hzdr.de/acredas, 2014.
(36) Zavarin, M.; Roberts, S. K.; Hakem, N.; Sawvel, A. M.; Kersting, A. B. Eu(III), Sm(III), Np(V), Pu(V), and Pu(IV) sorption to calcite. *Radiochimica Acta* **2005,** *93* (2), 93-102.
(37) Tits, J.; Wieland, E.; Bradbury, M. H.; Eckert, P.; Schaible, A. *The Uptake of Eu(lll) and Th(IV) by Calcite under Hyperalkaline Conditions.* ; PSI Bericht Nr. 02-03: Villigen, Switzerland, 2002.
(38) Lemire, R. J.; Fuger, J.; Nitsche, H.; Potter, P.; Rand, M. H.; Rydberg, J.; Spahiu, K.; Sullivan, J. C.; Ullmann, W. J.; Vitorge, P.; Wanner, H. *Chemical Thermodynamics of Neptunium and Plutonium*. Elsevier: Amsterdam, 2001; p 870.
(39) Guillaumont, R.; Fanghänel, T.; Fuger, J.; Grenthe, I.; Neck, V.; Palmer, D. A.; Rand, M. H. *Update on the chemical thermodynamics of uranium, neptunium, plutonium, americium and technetium. Chemical Thermodynamics Vol. 5*. OECD Nuclear Energy Agency: Elsevier, 2003; Vol. Vol. 5, p 960.
(40) Funke, H.; Scheinost, A. C.; Chukalina, M. Wavelet analysis of extended X-ray absorption fine structure data. *Physical Review* **2005,** *B 71*, 094110.
(41) Zachariasen, W. H. Crystal chemical studies of the 5f-series of elements: XII. New compounds representing known structure type. *Acta Crystallographica* **1949,** *2*, 388-390.
(42) Rothe, J.; Denecke, M. A.; Neck, V.; Muller, R.; Kim, J. I. XAFS investigation of the structure of aqueous thorium(IV) species, colloids, and solid thorium(IV) oxide/hydroxide. *Inorg Chem* **2002,** *41* (2), 249-258.
(43) Rothe, J.; Walther, C.; Denecke, M. A.; Fanghanel, T. XAFS and LIBD investigation of the formation and structure of colloidal Pu(IV) hydrolysis products. *Inorg. Chem.* **2004,** *43* (15), 4708-4718.
(44) Ikeda-Ohno, A.; Hennig, C.; Tsushima, S.; Scheinost, A. C.; Bernhard, G.; Yaita, T. Speciation and structural study of U(IV) and -(VI) in perchloric and nitric acid solutions. *Inorg. Chem.* **2009,** *48* (15), 7201-7210.
(45) Taylor, D. Thermal-expansion data. 2. Binary oxide with the fluorite and rutile structures, MO_2, and the antifluorite structure, M_2O. *Transactions and Journal of the British Ceramic Society* **1984,** *83* (2), 32-37.
(46) Hennig, C.; Ikeda-Ohno, A.; Emmerling, F.; Kraus, W.; Bernhard, G. Comparative investigation of the solution species $[U(CO3)_5]^{6-}$ and the crystal structure of $Na_6[U(CO3)_5]$ $12H_2O$. *Dalton Trans.* **2010,** *39* (15), 3744-3750.
(47) Clark, D. L.; Conradson, S. D.; Keogh, D. W.; Palmer, P. D.; Scott, B. L.; Tait, C. D. Identification of the limiting species in the plutonium(IV) carbonate system. Solid state and solution molecular structure of the Pu(CO3)(5) (6-) ion. *Inorg Chem* **1998,** *37* (12), 2893-2899.
(48) Guillaumont, R.; Fanghänel, T.; Fuger, J.; Grenthe, I.; Neck, V.; Palmer, D. A.; Rand, M. H. *Update on the Chemical Thermodynamics of Uranium, Neptunium, Plutonium, Americium and Technetium*. Elsevier: Amsterdam, 2003.
(49) Latta, D. E.; Gorski, C. A.; Boyanov, M. I.; O'Loughlin, E. J.; Kemner, K. M.; Scherer, M. M. Influence of Magnetite Stoichiometry on U-VI Reduction. *Environmental Science & Technology* **2012,** *46* (2), 778-786.
(50) Veeramani, H.; Scheinost, A. C.; Monsegue, N.; Qafoku, N. P.; Kukkadapu, R.; Newville, M.; Lanzirotti, A.; Pruden, A.; Murayama, M.; Hochella Jr., M. F. Abiotic reductive immobilization of U(VI) by biogenic mackinawite. *Environ. Sci. Technol.* **2013,** *47*, 2361-2369.
(51) Walther, C.; Denecke, M. A. Actinide Colloids and Particles of Environmental Concern. *Chemical Reviews* **2013,** *113* (2), 995-1015.
(52) Kersting, A. B. Plutonium Transport in the Environment. *Inorg Chem* **2013,** *52* (7), 3533-3546.
(53) Liger, E.; Charlet, L.; Van Cappellen, P. Surface catalysis of uranium(VI) reduction by iron(II). *Geochimica et Cosmochimica Acta* **1999,** *63* (19/20), 2939-2955.
(54) Husar, R.; Weiss, S.; Hennig, C.; Hübner, R.; Ikeda-Ohno, A.; Zänker, H. Formation of neptunium(IV)−silica colloids at near-neutral and slightly alkaline pH. *Environ. Sci. Technol.* **2015,** *49*, 665−671.